Available online at www.sciencedirect.com
ScienceDirect
Polymer 47 (2006) 8061–8071
polymer
www.elsevier.com/locate/polymer

Molecular modeling simulations and thermodynamic approaches to investigate compatibility/incompatibility of poly(L-lactide) and poly(vinyl alcohol) blends☆

Sheetal S. Jawalkar, Tejraj M. Aminabhavi*

Molecular Modeling Division, Center of Excellence in Polymer Science, Karnatak University, Pavate Nagar, Dharwad 580 003, Karnataka, India

Received 3 March 2006; received in revised form 1 September 2006; accepted 8 September 2006
Available online 2 October 2006

Abstract

This paper investigates the molecular modeling simulation approaches for understanding the blend compatibility/incompatibility of poly(L-lactide), PLL and poly(vinyl alcohol), PVA. Blends of PLL/PVA have been widely used in biotechnology as well as membranes in separation science. Realizing their importance, we thought of investigating to verify experimental observations on their compatibility/incompatibility aspects by calculating thermodynamic interactions between PLL and PVA over the entire range of blend compositions. In doing so, Flory–Huggins interaction parameter, χ, was computed for different blends using atomistic simulations to predict blend miscibility. It was found that at 1:9 blend composition of PLL/PVA, miscibility was observed, but increasing immiscibility was prevalent at higher compositions of PLL component. Computed results confirmed the literature findings on differential scanning calorimetry (DSC), Fourier transform infrared (FTIR) and mechanical property studies, suggesting the validity of modeling strategies. Plots of Hildebrand solubility parameter, δ, and cohesive energy density, CED, supported these findings. Miscibility of PLL and PVA polymers is attributed to hydrogen-bonding effect. Literature findings have been validated to understand the nature of interactions between different groups of the polymers by computing radial distribution function, RDF, for groups that are tentatively involved in such interactions, leading to miscibility or immiscibility. RDF plot was constructed to identify the exact contribution of particular atoms of polymers to confirm miscibility/immiscibility of blends. Results of this study are correlated well with the reported data. Kinetics of phase separation was examined using density profiles calculated from the MesoDyn approach to examine miscibility/immiscibility aspects of the blends. Computed free energy from the mesoscopic simulation of blends reached equilibrium, particularly when simulation was performed at higher time step, indicating the stability of the blend at certain compositions. X-ray diffraction profiles have been constructed for individual polymers as well as for their blends, which agreed well with the reported data.

Keywords: Poly(L-lactide); Poly(vinyl alcohol); Cohesive energy density

1. Introduction

Poly(L-lactide) (PLL), an aliphatic biodegradable polyester, has been widely used in drug delivery research [1–4]. It is generally prepared by ring-opening polymerization of lactide using the isomers like L-lactide and D-lactide. By controlling the amount of each isomer in the monomer feed, polymer tacticity can be manipulated [5]. In the polymer literature, considerable efforts have been made to modify the basic structure of PLL by copolymerization, grafting, etc., to improve its properties. Blending with another synthetic polymer such as poly(vinyl alcohol), PVA, could toughen PLL [6]. PLL has excellent tensile strength and modulus, with low glass transition temperature T_g of 65 °C and exhibits low carbon dioxide, oxygen and water vapor permeabilities [7]. Solubility parameter predictions indicated that PLL, having a polar chemical structure, is a good aroma barrier having a broad range of applications including packaging, textiles and composites

☆ This paper is CEPS communication # 116.

* Corresponding author. Tel.: +91 836 27715372; fax: +91 836 2771275.
E-mail address: aminabhavi@yahoo.com (T.M. Aminabhavi).

0032-3861/$ - see front matter © 2006 Elsevier Ltd. All rights reserved.
doi:10.1016/j.polymer.2006.09.030

[8–11]. On the other hand, PVA has been widely used in drug delivery [12,13] and membrane [14] applications. Blend compatibility studies on PLL and PVA have been recently reported by Shuai et al. [15], who suggested that PLL and PVA exhibit widely varying miscibility/immiscibility trends, depending upon their compositions.

In recent years, molecular modeling (MM) simulations have been advanced to such a level to predict the blend compatibility of polymers [16]. Of the several theoretical tools used to study polymer–polymer blend compatibility, mesoscopic dynamics [17,18] (MesoDyn) and dissipative particle dynamics (DPD) methods [19,20] have been widely used, wherein polymeric chains are treated in a coarse-grained (mesoscopic) level by grouping atoms together up to the persistence length of the polymers. MesoDyn is a dynamic mean-field density functional theory in which dynamics of phase separation is described by Langevin-type equations to study polymer diffusion. This method was successfully used for studying concentrated aqueous solutions of triblock copolymers [21] and employs soft interaction potentials allowing for large time-scale simulations. Time evolution of the system is obtained by solving Newton's equations of motion.

In continuation of our ongoing program of research on molecular mechanics (MM) and molecular dynamics (MD) calculations, we present here useful computational results that help to understand about the blend compatibility of PVA and PLL polymers. Earlier, Shuai et al. [15] suggested that PLL and PVA are not fully compatible at all blend compositions as evidenced by DSC and FTIR measurements. It is, therefore, important to validate the blend compatibility of PVA and PLL polymers over the practically useful range of compositions using an alternative methodology such as MD simulations. In this research, we have used both atomistic and mesoscopic level simulations to confirm blend compatibility/incompatibility aspects of PLL and PVA polymers to validate the experimentally reported data [15]. To the best of our knowledge, no such theoretical studies on these blends have been made earlier. Reported data from DSC and FTIR suggest that blends of PLL and PVA are immiscible at higher compositions of PLL (i.e., >30%), but miscibility is prevalent at lower compositions of PLL. It was confirmed that these polymers could mix only at 1:9 (wt/wt) ratio of PLL/PVA.

As reported before [15], the side –OH group of PVA is responsible to induce its miscibility with PLL, since PVA has the propensity to form hydrogen bonds with carbonyl group containing polymers, leading to blend compatibility. This aspect was further investigated by calculating the radial distribution function (RDF) on polymeric chains. DSC studies [15] also indicated a strong evidence of immiscibility of PLL and PVA blends at higher compositions of PLL, but blends are not completely miscible at all the compositions. Even though the reason for this behavior was not fully explored, literature data and our simulation results agree to the fact that the presence of C=O groups in PLL (MW = 800,000; $T_g = 65\ ^\circ C$; density = 1.206 g/cm^3) will restrict the free rotation around –C–C– bond of its backbone, which would hinder its chain mobility, resulting in its increased T_g. On the other hand, hydroxyl moiety of PVA (MW = 125,000; $T_g = 56.3\ ^\circ C$; density = 1.269 g/cm^3) is small compared to CH_3 and C=O groups in PLL and hence, it provides an ability to crystallize PVA much faster than PLL.

The present study seeks answers to these issues using MM and MD simulation techniques by treating hierarchically different lengths and time scales involved in the problem. MD simulations of the oligomers of polymers were performed at ambient temperature over wide range of compositions. Cohesive energy density, CED, of the pristine polymers in blends was determined to compute the solubility parameter, δ, of the blends as a function of blend composition. Flory–Huggins interaction parameter, χ, enthalpy, entropy and Gibbs free energy of mixing were also calculated to understand the energetics in mixing of polymers, which indicated favorable interactions. Interaction parameters obtained from atomistic simulations along with other structure-dependent (monomer number and length, characteristic ratio, etc.) parameters were subsequently supplied as input parameters to perform mesoscopic simulations. Short-scale characteristics were then absorbed into large structureless beads. Coarse-grained representation of the systems was then used to study the blends of high molecular weight and for extension of time scales that allowed the observation of phase separation. The degree of order (order parameter) of the phases formed was derived. These results indicated close agreements with the reported data of Shuai et al. [15], further strengthening the validity of the protocol employed in this study.

2. Computations and results

MD simulations were performed on the blends of PLL and PVA at ambient temperature (298 K) using MesoDyn and MesoDyn interfaces purchased from Accelrys, Inc., San Diego, CA, USA with the Material Studio Modeling (version 3.2) installed on Windows-2000. Flory's rotational isomeric state (RIS) model was used to describe the conformations of unperturbed chains [22]. For a good blending of PLL and PVA, amorphous phases were checked for space filling regularly after constructing the initial amorphous cell. If the chains of PLL and PVA were not well mixed (sufficient intermolecular contacts) in the initial configuration, then they were discarded and a new model was attempted. Bulk phases were generated on the amorphous cell after minimizing the initial structure using the conjugate gradient method (CGM), which utilizes the Polak–Ribiere algorithm with a convergence level of 0.001 kcal/mol/Å.

COMPASS [23] (condensed-phase optimized molecular potentials for atomistic simulation studies) force field based on PCFF (polymer consistent force field) was used for modeling interatomic interactions. In the COMPASS force field approach, total energy, E_T of the system was represented by the sum of bonding and non-bonding interactions given as:

$$E_T = E_b + E_0 + E_\phi + E_{oop} + E_{pe} + E_{vdw} + E_q \quad (1)$$

Here, the first four terms represent the bonded interactions, which correspond to energies associated with the bond, E_b, bond angle bending, E_0, torsion angle rotations, E_ϕ out of

loop, E_{oop} and potential energy, E_{pe}. Last two terms represent the non-bonded interactions, which consist of van der Waals term, E_{vdw} and electrostatic force, E_q. In COMPASS, E_{vdw} is invariably described by Lennard–Jones 6-12 potential, while electrostatic energy is calculated from the partial charges of atoms in the system as estimated by charge-equilibration method [24]. Electrostatic interaction was calculated by the well known Ewald summation method [25], since it accurately calculates the long-range interactions. The cell multi-pole method [26,27] was used to calculate the non-bonded interactions. This method is quite efficient to simulate big systems, since it scales linearly with the number of atoms, N (compared to cutoffs that scale as N^2) and requires a modest hardware memory. The periodic box is divided into M cubic cells with $M \cong N/4$. In each cell, the cells in the nearest neighborhood contribute to the near-field potential, while others to the far-field potential (short and long-range interactions). Interactions between atoms in the near-field cells are calculated directly for each pair of atoms. Interactions for atoms in the far-field cells are computed via expansions of multi-pole moments (charges, dipoles, quadrupoles and octupoles) around the center of each cell. Since it is assumed that interactions of atoms in the central cell with far-field atoms vary little from one atom position to another (compared to interactions between near-field atoms), Taylor coefficients of the expansions were calculated only for each cell and not for each atom. The schematic methodology used in our calculations is described in Fig. 1. Calculated solubility parameter values of individual polymers are given in Table 1.

For choosing polymer chain length in MD simulations, individual PVA and PLL polymers were subjected to minimization. Dynamics was performed to find δ plotted vs number of repeating units of the polymer. When a stable value of δ was obtained, it confirmed that the number of repeating units is sufficient for the simulation. In the present work, *syndiotactic* PVA of 21 units and PLL consisting of 10 repeating units were used to generate the amorphous cell of 1:1 blend. Density of the chosen polymers taken from the literature [28] were: $\rho_{(PVA)} = 1.269$ g/cm^3 and $\rho_{(PLL)} = 1.206$ g/cm^3. The system under investigation consisted of 242 atoms for 1:1 blend

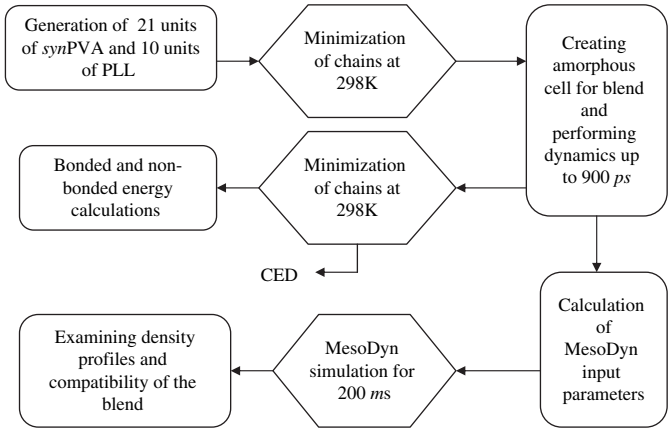

Fig. 1. Schematic representation of simulation procedure used to derive equilibrium structures of the blends.

Table 1
Repeating units, molecular weights and solubility parameters of PVA and PLL at 298 K

Polymer	Repeating units	Molecular weight	Solubility parameter (cal/cm^3)$^{0.5}$		
			Expt	COMPASS	GCM[a]
PLL	10	900	5.43 [10]	8.65	8.10
syn-PVA	21	924	12.60 [28]	11.02	10.03

[a] GCM – calculated by group contribution method, wherein molar attraction constants were taken from Ref. [28].

combination. Further, CED, δ and χ values were calculated. MD simulations under constant temperature and density (NVT ensemble) were performed for each configuration by using the Discover program of Accelrys. While running the dynamics, Anderson's stochastic method was used to control the temperature. A group-based cutoff of 8.5 Å with a spline width of 1 Å was applied to evaluate the non-bonded interactions, which owed to the separation between atoms.

Bulk amorphous states for pristine PLL or PVA and their blends were built using the cubic unit cells under periodic boundary conditions. Simulations were performed to build the systems with 3D periodicity and were equilibrated in the NVT ensemble at 298 K at which equilibration was usually achieved within 50 ps with the dynamics that was followed by data accumulation run lasting up to 900 ps with configurations saved every 100 ps. The fluctuation profiles in the bonded and non-bonded energies during MD simulations are shown in Fig. 2. The snapshot unit cell (CPK model) for all blend ratios of PVA/PLL is shown in Fig. 3. Here, carbon atoms are grey, hydrogen white and oxygen red in color. (For interpretation of the references to color, the reader is referred to the web version of this article.) Detailed model construction protocol is described by taking different ratios of the number of chains of PLL to the number of chains of PVA in the unit cells. The number of chains per unit cell, chain length and density values are summarized in Table 2. Density of the blends was calculated from the density of individual polymers and volume fraction of each polymer. Usually, the initial amorphous structure is in a relatively high-energy state, but before performing MD calculations, energy minimization was done to bring the system close to minimum. Here, the simulation time depends upon the number of atoms in the system; simulation was performed until the total energy of the system was stabilized. The last few hundred ps of the trajectory files were used to calculate δ, defined as the square root of CED, as well as the Flory–Huggins [29] parameter, χ, given by:

$$\chi = \frac{z\Delta E_{mix}}{RT} \tag{2}$$

Here, z is the coordination number (its value for cubic lattice model is taken as 6), R is the molar gas constant (cal/mol) and T is the temperature in kelvin, at which simulation was performed. Energy of mixing, ΔE_{mix}, needed to compute χ was calculated as:

$$\Delta E_{mix} = \phi_A \left(\frac{E_{coh}}{V}\right)_A + \phi_B \left(\frac{E_{coh}}{V}\right)_B - \left(\frac{E_{coh}}{V}\right)_{mix} \tag{3}$$

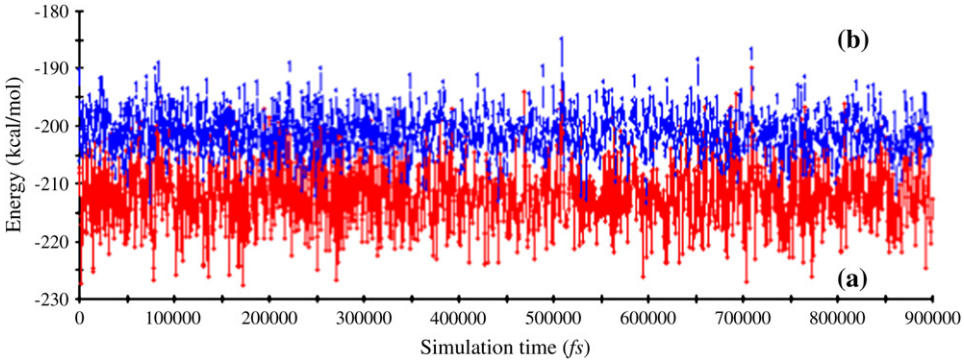

Fig. 2. Plot of (a) potential energy and (b) non-bond energy fluctuations vs simulation time (fs) during MD calculation.

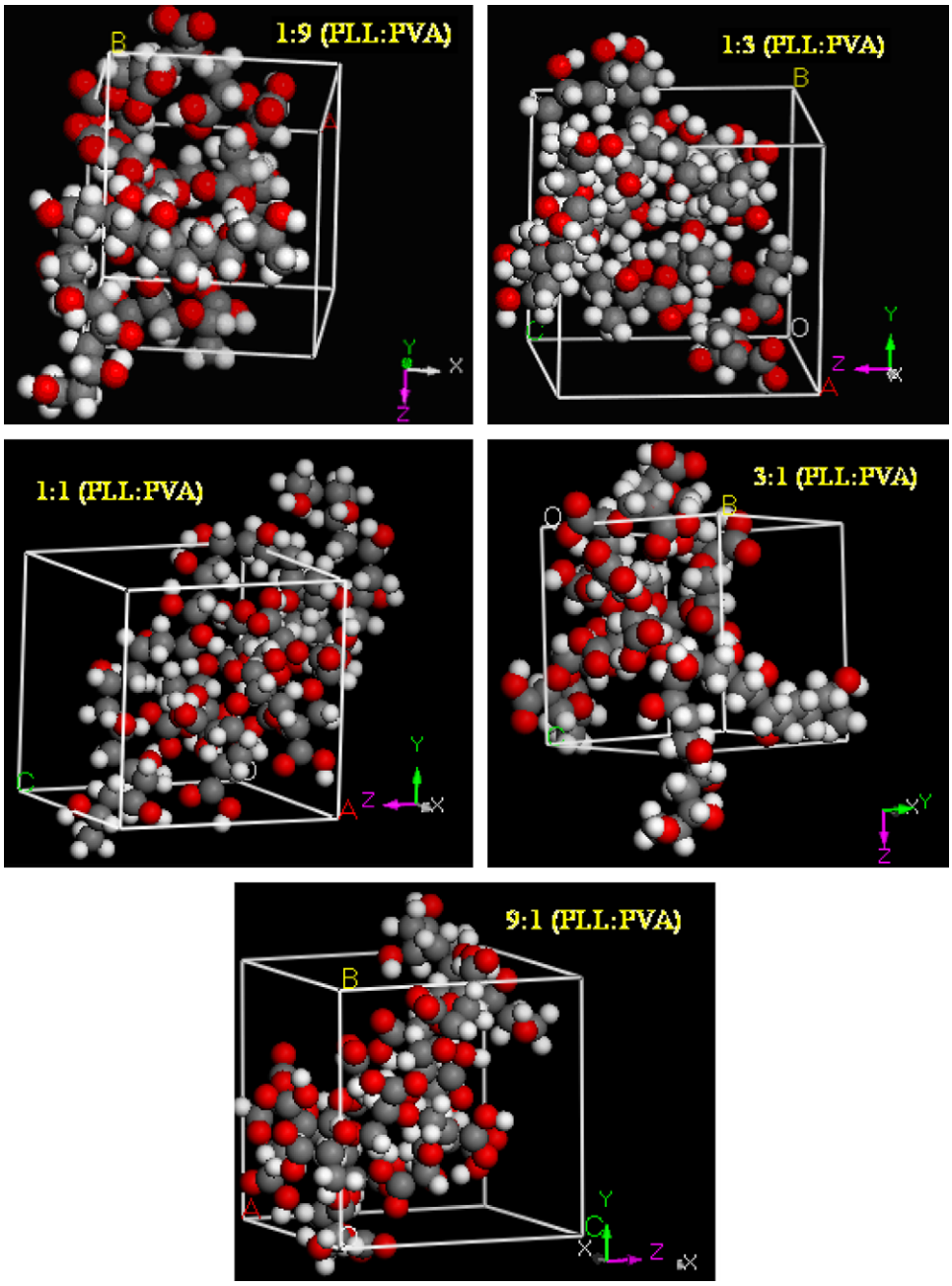

Fig. 3. A typical snapshot of blends of PVA/PLL displayed in the CPK model (Corey–Pauling–Koltun model), where the radius is dependent on van der Waals radius of the element.

Table 2
Simulated data of PVA/PLL blends for different compositions at 298 K

System no.	Blend ratio in unit cell	Composition (wt% PLL)	Density (g/cm^3)	Molar volume (cm^3/mol)	χ (Eq. (2))
1	1PVA chain	0	1.2690	728	N/A
2	1PLL chain	100	1.2060	746	N/A
3	1:9 (PLL/PVA)	10	1.2627	771	0.134
4	1:3 (PLL/PVA)	25	1.2533	761	0.270
5	1:1 (PLL/PVA)	50	1.2375	737	0.363
6	3:1 (PLL/PVA)	75	1.2218	750	0.654
7	9:1 (PLL/PVA)	90	1.2123	758	0.540

N/A – not applicable.

Here, the subscripts A, B and mix represent CED values of PLL, PVA and PLL/PVA blends, respectively, by considering the identity: CED $\equiv E_{coh}/V$. The symbols ϕ_A and ϕ_B represent the volume fractions of PLL and PVA, respectively. Using the calculated value of energy of mixing for PLL and PVA, χ was calculated from Eq. (2). Further, by using the Discover minimization, an input file was generated for structures in which the vibrational analysis mode was carried out in addition to optimization. Here, the vibrational intensities for FTIR spectra were obtained and plotted against frequency to find the peaks of different groups of the polymer.

The computed values of different energy components of Eq. (1) are summarized in Table 3. Due to computer data-storage space limitations, simulations could not be performed using the actual size of the polymers and hence, size of the polymer used in model calculations is important while computing thermodynamic quantities to understand what minimum level molecular size is sufficient to represent the real polymer coil. To determine this minimum size, solubility parameters of PLL and PVA at the chosen molecular weights were computed until any further increase in polymer molecular weight did not change the solubility parameter values. As shown in Fig. 4, the solubility parameter of PLL levels off when the number of repeating units of PLL exceeds 10 (i.e., MW > 900). Similar findings were observed for poly(ether imide) and poly(carbonate) blends studied by Zhang et al. [30], wherein it was found that 10 repeating units for polycarbonate were sufficient to perform the simulation. It may be noted that Fan et al. [31], used 21 repeating units of polycarbonate to achieve the simulation. In a similar fashion, δ vs number of repeating units of PVA as shown in Fig. 5, for chain extensions up to 50 monomer units, suggests that δ did not vary much beyond 20 monomer units.

Table 3
Computed energy values (kcal/mol) for PVA/PLL blends

System no.[a]	$E_{potential}$	E_{bond}	$E_{torsion}$	$E_{bond\ angle}$	E_{vdw}	E_{es}	E_{oop}
3	−929	−0.03	−247	−1.9	−28	−687	0.03
4	−677	0.18	−195	−2.8	−31	−867	0.09
5	−387	0.11	−160	−4.5	−39	−250	0.26
6	−74	0.15	−138	−5.8	−56	−30	0.00
7	−239	−0.21	−91	−6.5	−70	−339	0.41

[a] System nos. refer to blends given in Table 2.

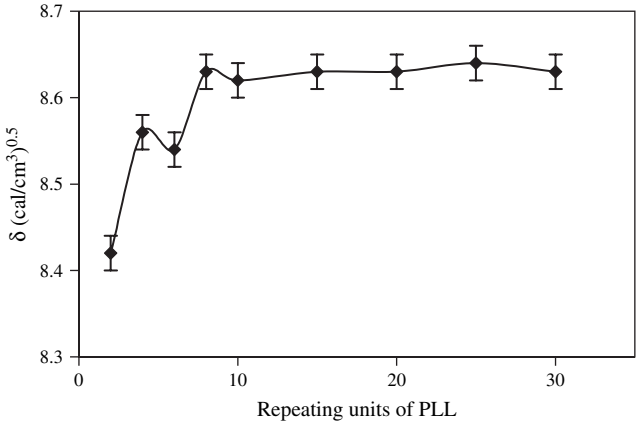

Fig. 4. Computed solubility parameters of PLL vs number of repeating units of PLL.

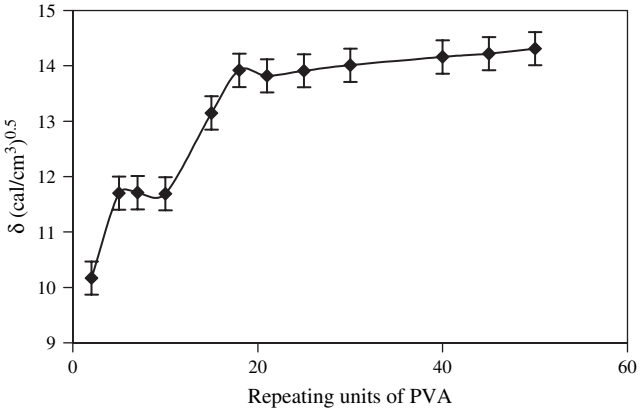

Fig. 5. Computed solubility parameters of PVA vs number of repeating units of PVA.

3. Blend compatibility/incompatibility

In the present study, the tendency of PVA and PLL polymers to mix at a specific composition was estimated by calculating CED of the blends and pure polymer components. To understand the miscibility/immiscibility behaviors of PLL and PVA, the critical value of χ was calculated using the equation:

$$(\chi_{AB})_{critical} = \frac{1}{2}\left(\frac{1}{\sqrt{m_A}} + \frac{1}{\sqrt{m_B}}\right)^2 \quad (4)$$

where m_A and m_B are degrees of polymerization (actual number of repeating units) of A and B. Blends are miscible if $\chi_{AB} < (\chi_{AB})_{critical}$ and vice versa. For a miscible blend, Gibbs free energy, ΔG_m is negative. If χ_{AB} is considerably greater than the critical value, then blends are immiscible. For a value of χ_{AB} greater than the critical value (i.e., $(\chi_{AB})_{critical}$), the blends are partially miscible. Thus, comparing the measured χ_{AB} with the critical value provides a good indication about the extent of blend miscibility. Therefore, we have used χ_{AB} rather than enthalpy of mixing, ΔH_m to investigate the miscibility of PLL and PVA blends. The results of χ vs weight

fraction of PLL calculated from Eqs. (2) and (4) are displayed in Fig. 6. Fig. 7 displays the variation of CED with weight fraction of PLL, wherein immiscibility is exhibited by the minima observed at 1:1 blend composition. Notice that $\chi_{critical}$ calculated from Eq. (4) exhibits a linearity over the studied composition range of the blends, whereas χ values calculated from Eq. (2) increase steadily from 0.134 to 0.654 and then decline to 0.540. In the case of 1:9 PLL/PVA blend system, the simulated value of χ is slightly below the $\chi_{critical}$ line as shown in Fig. 6, thus showing a slight miscibility of the blend. For 1:3, 1:1, 3:1 and 9:1 compositions of PLL/PVA blends, χ values are all above the $\chi_{critical}$ line, indicating immiscibility of PLL and PVA blends. This is also in conformity with the reported data of the literature [15].

To understand the phenomenon thermodynamically, enthalpy of mixing, ΔH_{mix}, was calculated:

$$\Delta H_m = V_m \left\{ (CED_A)^{0.5} - (CED_B)^{0.5} \right\}^2 \phi_A \phi_B \quad (5)$$

Here, V_m is the total volume of the blend. CED values used in computing ΔH_m were taken from the MD simulations, suggesting that both PLL and PVA are immiscible at all compositions (viz., 1:3, 1:1, 3:1 and 9:1) except at 1:9 composition of PLL/PVA. From Table 3, it can be seen that large negative energy values of the potential energy term contribute to miscibility of the blend, while lesser negative energy values from other contributions of Eq. (1) tend to drive the blend away from miscibility. The value of $\chi_{critical}$ is around 0.143, which is indeed a demarcation line for the blend to be miscible. Notice that the concentration dependence of χ computed by the simulation procedure (see Fig. 6) exhibits the same trend as the concentration dependence of melting temperature, T_m of the PLL-rich phase [15]. The change in concentration is mainly originated from van der Waals and electrostatic energy terms. However, the widely varying values of χ from 0.134 to 0.654 are attributed to partial miscibility of the blends, since no specific interactions between PLL and PVA exist. Thus, entropy effects may have a significant influence, but these were not included in the MD calculations. Notice that for a blend to be miscible, large negative contributions from $E_{potential}$, $E_{torsion}$, E_{vdw} and E_{es} are observed as can be seen in Table 3.

After fixing the atoms for 1:1 blend composition, other compositions viz., 1:9, 1:3, 3:1 and 9:1 of the blends of PLL/PVA were also studied to see if they are miscible or not. The time required to attain such equilibria depends upon the size of the system as determined by running the simulation until complete minimization. Once the average total energies were obtained for the system, then ΔH_m was calculated for each blend system using Eq. (5). To compute the free energy of mixing, ΔG_m, we needed the entropy of mixing term, ΔS_m^{comb}, which was obtained from the combinatorial entropy term of the binary blends using Flory–Huggins theory [22,29]:

$$\Delta S_m^{comb} = -R[x_A \ln x_A + x_B \ln x_B] \quad (6)$$

Here, x_A and x_B are the mole fractions of A and B. Then, by using the identity: $\Delta G_m = \Delta H_m - T\Delta S_m^{comb}$, Gibbs free energy of mixing was computed. Notice that in Fig. 8, both ΔG_m (dotted curve) and ΔH_m exhibit almost similar trends over the entire compositions of PLL of the blend. These curves display the maxima at 1:1 blend composition. This observation is substantiated by the minima observed at 1:1 blend composition in the plot of CED vs weight fraction of PLL (see Fig. 7).

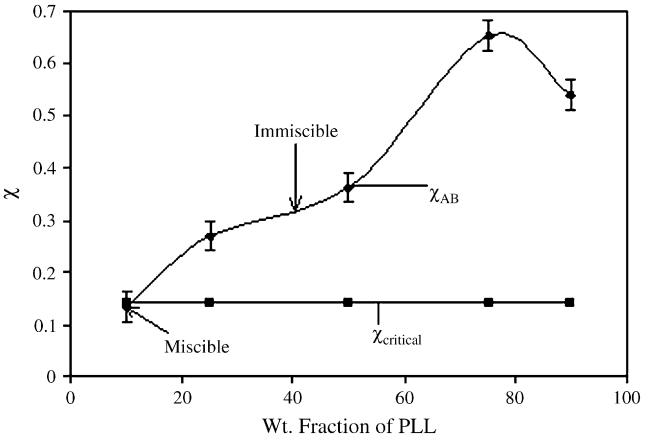

Fig. 6. Flory–Huggins interaction parameter vs weight fraction of PLL.

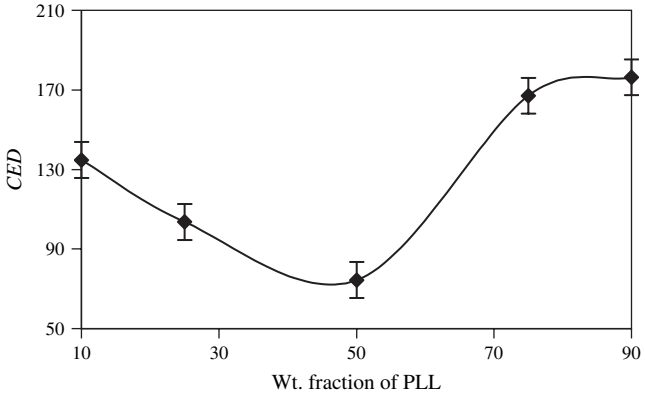

Fig. 7. Cohesive energy density vs weight fraction of PLL.

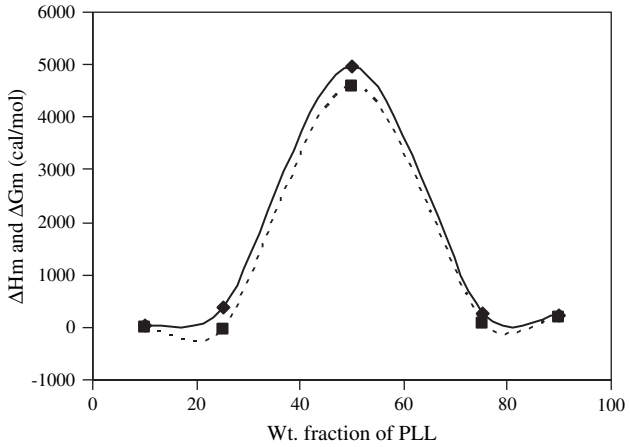

Fig. 8. Molar enthalpy (solid curve) and Gibbs free energy (dashed curve) vs weight fraction of PLL.

4. Model validation of the reported experimental data

In order to further probe into the details of understanding PLL and PVA blend miscibility/immiscibility aspects, MesoDyn program incorporated in Accelrys package, was used to simulate the phase separation dynamics of the blends at the mesoscopic level. This approach is based on the dynamic variant of the mean-field density functional theory [18], which is similar to the classical dynamic random phase approximation (RPA) [32]. Here, the polymer chains are modeled as ideal Gaussian chains consisting of beads, each representing the monomer of a polymer (Kuhn statistical segment). Then, free energy of the system can be calculated in terms of the bead distribution functions. Bead positions are then correlated to each other by converting it to a many-body problem. In these calculations, the inter-chain correlations were neglected and the system was approximated by a set of independent Gaussian chains embedded in the mean-field. Detailed mathematical derivations have been given earlier [16] along with the procedures involved in solving the equations. The equation for the calculation of MesoDyn chain length (N_{Meso}) is given as:

$$N_{\text{Meso}} = \frac{M_{\text{p}}}{M_{\text{m}} C_{\text{n}}} \tag{7}$$

where M_{p} is polymer molecular weight, M_{m} is monomer molecular weight and C_{n} is characteristic ratio. The MesoDyn input parameter is related to Flory–Huggins χ parameter through the equation:

$$\nu^{-1}\varepsilon_{ij} = \chi_{ij} \text{R}T \tag{8}$$

where χ_{ij} is taken from atomistic simulations performed on each blend system at each composition (as discussed before), R is molar gas constant (cal/mol) and T is 298 K. The N_{Meso} and $\nu^{-1}\varepsilon_{ij}$ (interacting energies between pair of interacting bead types) are used as the input parameters for MesoDyn calculations. For 1:1 (PLL/PVA) blend system, N_{Meso} taken for PLL and PVA were 0.41 and 0.52 units, respectively, and $\nu^{-1}\varepsilon_{ij}$ was 6.2 kJ/mol.

To account for numerical stability, time step for the simulation was chosen in such a way that the dimensionless time step, τ used in the program was 0.5 (i.e., between 0 and 1) and bond length was taken to be 1.154 nm throughout. Thus, 200 μs was the time step used for all compositions of PLL/PVA blend. A constant noise parameter of 75.002 was maintained for the entire simulation, since too high or too low value will lead to system unstability [33], which was applied to shorter chains with longer statistical units [16]. The grid dimensions were chosen to be $32 \times 32 \times 32$ nm and the size of the mesh over which density variations are to be plotted in MesoDyn length units using the Grid spacing field was 1 nm. Bond length was 1.1543 Å times the cell length to guarantee isotropy of all the grid-restricted operators. Flory–Huggins χ parameter was calculated at 298 K for the total simulation time of 200 μs. Non-ideality of the system was then incorporated through the effective external potentials, which were obtained from χ parameter for pair of species chosen. After calculating the energy of mixing using the atomistic simulation, it was related to Flory–Huggins χ parameter as:

$$\chi = \left(\frac{\Delta \tilde{E}_{\text{mix}}}{\text{R}T}\right) V_{\text{mon}} \tag{9}$$

In the mesoscopic simulation, after setting up the initial configurations, the systems were let to evolve towards equilibrium (phase separation or mixing). The initially homogeneous phases were cooled in a two-phase region by turning on the interactions at time, $t = 0$. Then, the kinetics of phase separation was examined first and blend compatibility was deduced from the final equilibrium morphologies.

In order to validate the reported data [15], the kinetics of phase separation in the blends was also investigated by calculating the structure factor, $S(q,t)$ [where q is scattering vector equal to $(4\pi/\lambda)\sin(\theta/2)$; λ and θ are wavelength of light and scattering angle, respectively] at regular time intervals [34]. The intensity was plotted vs q as shown in Fig. 9, where all the three patterns viz., for pristine PVA, PLL and 1:1 blend of PLL/PVA (typical case) were obtained. It was observed that maximum peak has moved towards smaller q, but to calculate X-ray scattering curve for an amorphous system, we required all atoms of the system as input; these calculations were performed either on a single configuration or on a series of configurations. The actual computation utilizes Debye formula [35] to produce scattering curves with appropriate rigorous modifications. However, the output results are the values of intensity vs the scattering angle or scattering vector, q. The scattering curve, $I(q)$, for the polymer chain, which is related through Fourier transform operation to radial distribution function was calculated as:

$$I(q) = \sum_j \sum_k \frac{\left[f_i f_k (\sin q r_{jk})\right]}{q r_{jk}} \tag{10}$$

where q denotes the indices j and k extending over all atoms in the entire polymer chain and experimental $I(q)$ was used to validate the force field.

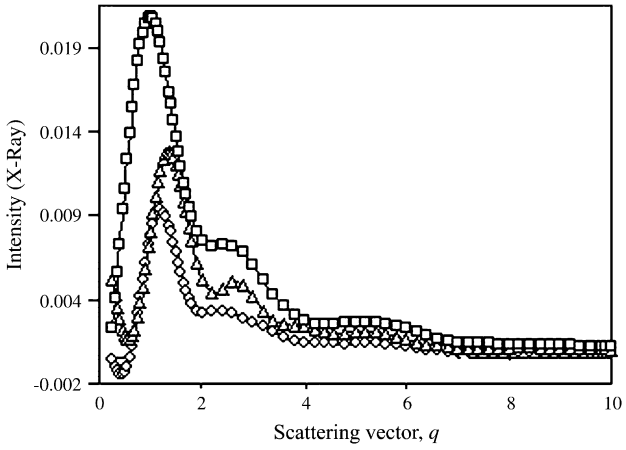

Fig. 9. X-Ray scattering profile of PLL (□), pristine PVA (△) and PLL/PVA (○) blends.

Reported experimental DSC thermograms by Shaui et al. [15] suggested two isolated T_g corresponding to PLL-rich and PVA-rich phases suggesting that PLL is not miscible with *syndiotactic* PVA over the entire composition range. However, for the solution casted PVA/PLL blend films, the enthalpy corresponding to PVA phase in its blends with PLL was constant and remained composition independent. In case of PVA/PLL blends, no change on blend composition was observed in χ_{AB} values of PLL phase when PLL content was >70%. For PLL/PVA blends with PLL contents less than the critical value of 70%, a larger depression in T_m was observed for the PLL phase because PLL is immiscible with PVA. However, at low PLL contents, the interaction between PVA and PLL segments is higher and hence, blends are miscible. Thus, the compatibility of PLL with PVA increased at lower contents of PLL. Experimental FTIR and XRD studies have also confirmed that tacticity of PVA has either none or only negligible effect on the crystallization of the blends [15].

Radial distribution function (RDF) [designated by the symbol, $g(r)$] between different types of possibly interacting pairs of atoms was computed from the trajectory coordinates. The $g(r)$ measures the point probability of finding one of the atoms at a distance, r from the other atom. Experimentally, measurement of $g(r)$ has been used to study the changes in local packing of polymer glasses, which occur during physical aging process making the material brittle in the absence of chemical degradation [36]. To perform the RDF calculations, we have considered the interactions between oxygen atom of carbonyl group of PLL with hydrogen atoms of hydroxyl groups of PVA. For a pair of atoms, A and B, the $g_{AB}(r)$ function is calculated as:

$$g_{AB}(r) = \frac{\langle n_{AB}(r)\rangle}{4\pi r^2 \Delta r \rho_{AB}} \tag{11}$$

where $\langle n_{AB}(r)\rangle$ is the average number of atom pairs between r and $r+\Delta r$ and ρ_{AB} is the density of atom pairs of type AB. Here, $g(r)$ is utilized to distinguish between amorphous and crystalline structures. RDF functions have been calculated for various pairs of atoms of molecules for three types of contributions viz., total, intermolecular and intramolecular. RDF can thus provide an insight as to how the atoms pack in an amorphous structure. Fig. 10 displays the total pair distribution function as a function of r for the bulk simulated structures, wherein one can see the variation of $g_{AB}(r)$ for the backbone containing carbon–carbon atoms of the simulated structures of PVA and PLL. Peaks of $g_{AB}(r)$ indicate the presence of definite correlation between atoms within that radius, while the absence of any peaks beyond 4 Å distance indicates that there is no long-range order in the systems. At long distances, $g_{AB}(r)$ approaches unity, which is quite probable for a purely amorphous system. However, the peaks observed at distances less than 4 Å are assigned to a specific distance of the closely coupled atoms. RDF study performed for 1:1 blend of PLL/PVA produced a peak for oxygen atom of PLL within 4 Å and two peaks for hydrogen atom of PVA, one at 2.5 Å and the other beyond 4 Å, as shown in Fig. 10. This indicates that there are more interactions with the oxygen atom, while there is less interaction with the hydrogen atoms of PVA. Even though the blend is amorphous, there is a sharp peak for oxygen within 4 Å and hydrogen bonding in the blend is weak, indicating immiscibility for this blend. Therefore, C=O group is responsible for observed little miscibility among all the ratios of PLL/PVA blends.

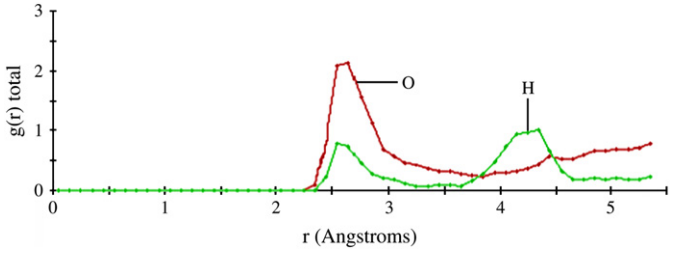

Fig. 10. Plot of radial distribution function [pair correlation function, $g(r)$] computed for oxygen atoms of carbonyl group of PLL in relation with the hydrogen atoms of PVA.

The inter-hydrogen bonding between OH groups of PVA and carbonyl group of PLL was reported earlier by FTIR [15]. Detectable frequency shifts for ester carbonyl group of PLL were not observed in PVA/PLL blends with >50% of PLL due to the absence of inter-polymer hydrogen bond or weak hydrogen bond interactions between the polymers. However, the shoulder peak got shifted to a lower wave number when PLL is <50% in the blend, which becomes more intense due to which the characteristic carbonyl absorption band broadened towards lower frequency range in the blends containing lower amount of PLL. Such a shift in shoulder to lower wave number confirmed the formation of new inter-polymer hydrogen bonding in blends containing <50% of PLL [15]. Simulated FTIR results on PLL and PLL/PVA blend (3:1) have shown a carbonyl absorption band in the region 1716 cm^{-1} and 1719 cm^{-1}, respectively, which got shifted to lower wave number for blends containing lower amount of PLL (i.e., PLL/PVA ratio of 1:3), which appeared around 1682 cm^{-1}.

In MD simulations, it is important to realize the system stability before one gets accurate and reliable data. The MD simulations on free energy, which asymptotically approached a stable value when the system attains dynamic equilibrium,

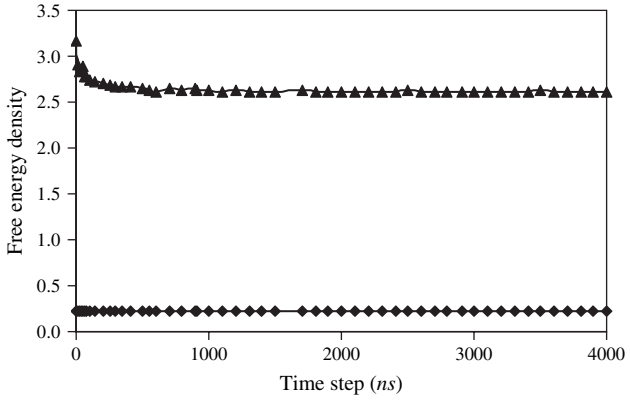

Fig. 11. Plot of free energy density vs time step for 1:3 blend of PLL/PVA for 200 μs simulation time.

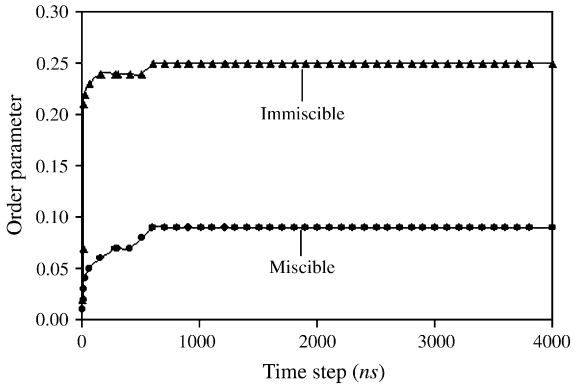

Fig. 12. Mesodynamic order parameter for 1:1 (PLL/PVA) blend as a function of time step (ns).

but free energy density is not routinely calculated for real systems and hence, its direct comparison with experimental data was not possible. At any rate, the evolution of free energy is a good measure of stability of a blend system. The plot of free energy density vs time step given in Fig. 11 shows that the system reached equilibrium when it was simulated for higher time interval, indicating its stability.

The order parameter, P_i, defined as the volume average of the difference between local density squared and the overall density squared, is given by the integral,

$$P_i = \frac{1}{V}\int_V \left(\eta_i^2(r) - \eta_i^2\right) dr \tag{12}$$

where η_i is dimensionless density (volume fraction) of the species, i. This is an important parameter, which when plotted as

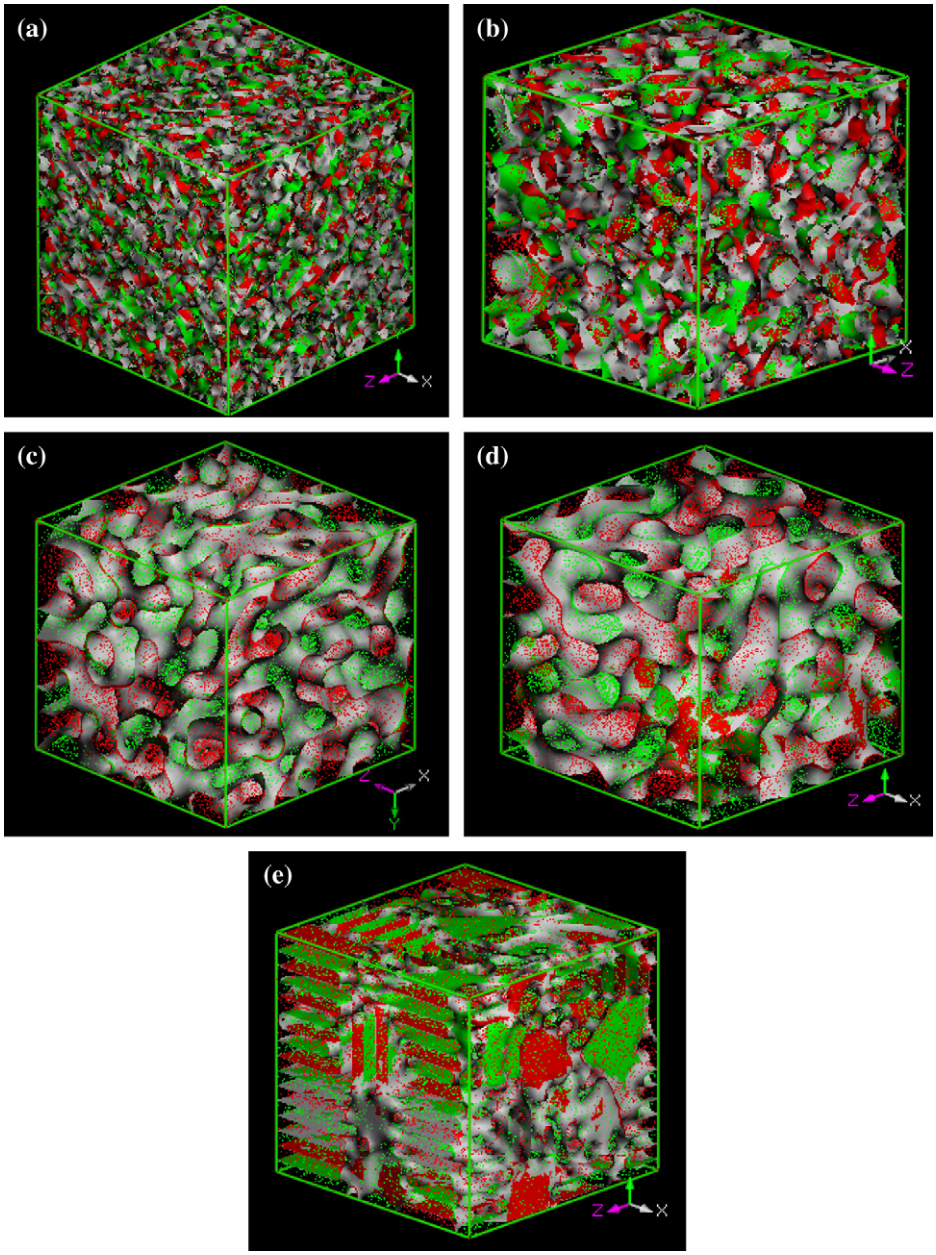

Fig. 13. Mesophase density profiles of (a) 1:9, (b) 1:3, (c) 1:1, (d) 3:1 and (e) 9:1 PLL/PVA blends.

a function of time step, to understand the miscibility/immiscibility aspects of polymeric blends. Fig. 12 shows the plot of order parameter for 1:1 PLL/PVA blend. Order parameters with large values indicate strong phase segregation, which is observed for 1:3, 1:1, 3:1 to 9:1 blends. However, very small values at the initial time step from 0 ns onwards indicate blend miscibility for 1:9 composition of PLL/PVA. As seen from Fig. 12, for systems 3–7 (Table 3), order parameter is >0.1, indicating blend immiscibility, whereas for 1:9 blend of PLL/PVA, its value is <0.1, indicating their miscibility. This is further sustained by the construction of density profiles for all blend systems, which clearly showed the phase separation (see that the extent of two polymers, red and green slices are well separated from Fig. 13 with the well-defined interfaces) computed for 200 μs simulation times. (For interpretation of the references to color, the reader is referred to the web version of this article.) Usually, phase separation proceeds through the diffusion of component polymers at the interfaces, but at later stages, phase separation barrier occurs due to diffusion. Notice that Fig. 13(a) confirms the miscibility of two phases for 1:9 PLL/PVA blend. Density profile pictures shown in Fig. 13(b)–(e) are indicative of blend immiscibility at high PLL content. Particularly, in Fig. 13(e), one can see the total immiscibility. This validates the reported data as well as the results obtained from atomistic simulations, discussed before.

To strengthen the above discussions, it is useful to look at the mechanical property data. Tensile strength and elongation at break data on PVA/PLL blends reported before [15] suggested an agreement with the present calculations to predict miscibility/immiscibility trends. Both tensile strength and elongation at break were reported to increase with increasing PVA content, i.e., at lower amounts of PLL, especially for the blend containing 10% PLL. The existence of two isolated and constant T_g values that were independent of the blend composition indicates that PLL and PVA are immiscible in the amorphous region. Also, see the computed X-ray plots in Fig. 9. However, the DSC data demonstrated [15] the presence of some degree of compatibility related to the composition in PLL/PVA blend. The formation of inter-polymer hydrogen bonding in the amorphous region, which is regarded as the driving force, leading to some degree of component compatibility in immiscible systems, has been confirmed by DSC and FTIR data, especially for blends containing lower PLL contents [15].

5. Conclusions

The reported data on blend compatibility studies of PLL and PVA polymers have been validated using the COMPASS force field and MD simulation protocols. Atomistic and mesoscopic simulations confirmed the reported experimental data to understand about compatibility/incompatibility of the blends. It was found that blends are miscible above 25 wt% composition of PLL, while for other compositions, these are immiscible. These findings are based on the computed values of χ for blends, which were 0.143, i.e., below the $\chi_{critical}$ value as was observed in case of 1:9 PLL/PVA blend system; this indicated their slight miscibility, suggesting that atomistic simulation methodology has agreed well with the mesoscopic simulation protocols. From the peak obtained by RDF we find that the C═O group is responsible for the little miscibility occurring at low PLL content of the blend. The value of order parameter being <0.1 further supported the miscibility of PLL and PVA polymers below 25 wt% of PLL in the blend. Mesoscopic density slices confirmed the phase separations between PLL and PVA polymers above 25% PLL of the blend. In conclusion, we have confirmed that 1:9 blend of PLL/PVA is miscible because χ is smaller than $\chi_{critical}$ whereas, at other compositions, these blends are immiscible. MesoDyn computations supported this observation by clearly showing the phase separation between the computer generated density profiles. The present results could successfully validate the reported experimental observations on the compatibility/incompatibility aspects of PLL/PVA blends.

Acknowledgements

The authors thank the University Grants Commission (UGC), New Delhi, India for a major funding (F1-41/2001/CPP-II) to establish Center of Excellence in Polymer Science at Karnatak University, Dharwad. We also thank Mr. Ashok Betraj (Apsara Innovations, Bangalore, India), Mr. Anand Gupta (Accelrys Inc., San Diego, CA, USA), and Dr. M. Mori (Accelrys Inc., Japan) for their helpful discussions during the course of this research.

References

[1] Anderson KS, Lim SH, Hillmyer MA. J Appl Polym Sci 2003;89:3757.
[2] Fayt R, Jerome R, Teyssie P. J Polym Sci Part B Polym Phys 1989;27:775.
[3] Muratoglu OK, Argon AS, Cohen RE. Polymer 1995;36:4771.
[4] Yu ZZ, Ou YC, Hu GH. J Appl Polym Sci 1998;69:1711.
[5] Wang Y, Hillmyer MA. J Polym Sci Part A Polym Chem 2001;39:2755.
[6] Kim HC, Nam KH, Jo WH. Polymer 1993;34:4043.
[7] Mainil-Varlet P, Curtis R, Gogolewski S. J Biomed Mater Res 1997;36:360.
[8] Dattaa R. FEMS Microbiol Rev 1995;16(2/3):221.
[9] Drumright RE, Gruber PR, Henton DE. Adv Mater 2000;12:1841.
[10] Ikada Y, Tsuji H. Macromol Rapid Commun 2000;21:117.
[11] Lehermeier HJ, Dorgan JR, Way D. J Membr Sci 2001;190(2):243.
[12] Kurkuri MD, Aminabhavi TM. J Controlled Release 2004;96:9.
[13] Kumbar SG, Aminabhavi TM. J Appl Polym Sci 2001;84:552.
[14] Yu J, Lee CH, Hong WH. Chem Eng Process 2002;41:693.
[15] Shuai X, He Y, Asakawa N, Inoue Y. J Appl Polym Sci 2001;81:762.
[16] Jawalkar SS, Adoor SG, Sairam M, Mallikarjuna NN, Aminabhavi TM. J Phys Chem B 2005;109:15611.
[17] Fraaije JGEM. J Chem Phys 1993;99:9202.
[18] Fraaije JGEM, van Vlimmeren BAC, Maurits NM, Postma M, Evers OA, Hoffman C, et al. J Chem Phys 1997;106:4260.
[19] Groot RD, Warren PB. J Chem Phys 1997;107:4423.
[20] Groot RD, Madden TJ. J Chem Phys 1998;108:8713.
[21] van Vlimmeren BAC, Maurits NM, Zvelindovsky AV, Sevink GJA, Fraaije JGEM. Macromolecules 1999;32:646.
[22] Flory PJ. Statistical mechanics of chain molecules. Munich, Germany: Hanser; 1989.
[23] Rigby D, Sun H, Eichinger BE. Polym Int 1997;44:311.

[24] Rappe AK, Goddard WA. J Phys Chem 1991;95:3358.
[25] Ewald PP. Ann Phys 1921;64:253.
[26] Schmidt KE, Lee MA. J Stat Phys 1991;63:1223.
[27] Ding HQ, Karasawa N, Goddard III WA. J Chem Phys 1992;97:4309.
[28] Grulke EA. Solubility parameter values. In: Brandrup J, Immergut EH, editors. Polymer handbook. 4th ed. New York: Wiley; 1999.
[29] Flory PJ. Principles of polymer chemistry. Ithaca, New York: Cornell University Press; 1953.
[30] Zhang M, Choi P, Sundararaj U. Polymer 2003;44:1979.
[31] Fan CF, Cagin T, Chen ZM, Smith KA. Macromolecules 1994;27:2383.
[32] de Gennes PG. Scaling concepts in polymer physics. Ithaca, New York: Cornell University; 1979.
[33] Spyriouni T, Vergalati C. Macromolecules 2001;34:5306.
[34] Groot RD, Madden TJ, Tildesley DJ. J Chem Phys 1999;110:9739.
[35] Debye PW. Ann Phys 1915;46:809.
[36] Roe RJ. Glass transition, Encyclopedia of polymer science and engineering. New York: John Wiley and Sons, Inc.; 1988.